Developmental Biology **236,** 165–180 (2001)
doi:10.1006/dbio.2001.0315, available online at http://www.idealibrary.com on IDEAL®

The Zinc Finger Protein DIE-1 Is Required for Late Events during Epithelial Cell Rearrangement in *C. elegans*

Paul J. Heid,*,[1] William B. Raich,†,[2] Ryan Smith,† William A. Mohler,‡,[3] Kristin Simokat,† Steven B. Gendreau,*,[4] Joel H. Rothman,*,[5] and Jeff Hardin†,[6]

**Department of Biochemistry, †Program in Cellular and Molecular Biology, and ‡Laboratory of Molecular Biology, University of Wisconsin, Madison, Wisconsin 53706*

The mechanism by which epithelial cells undergo directed rearrangement is central to morphogenesis, yet the regulation of these movements remains poorly understood. We have investigated epithelial cell rearrangement (intercalation) in the dorsal hypodermis, or embryonic epidermis, of the *C. elegans* embryo by analyzing the *die-1(w34)* mutant, which fails to undergo normal intercalation. Dorsal hypodermal cells of *die-1(w34)* homozygous embryos initiate but fail to complete the process of intercalation. Multiphoton microscopy reveals that intercalating cells extend monopolar, basolateral protrusions in their direction of migration; posterior dorsal hypodermal cells in *die-1(w34)* mutants appear to extend protrusions normally, but fail to translocate their cell bodies to complete rearrangement. Despite abnormal intercalation, the subsequent morphogenetic movements that enclose the embryo with epithelial cells and the process of dorsal cell fusion still occur. However, elongation of the embryo into a wormlike shape is disrupted in *die-1(w34)* embryos, suggesting that intercalation may be necessary for subsequent elongation of the embryo. Actin filaments are not properly organized within the dorsal hypodermis of *die-1(w34)* embryos, consistent with intercalation's being a necessary prerequisite for elongation. The *die-1* gene encodes a C2H2 zinc finger protein containing four fingers, which likely acts as a transcriptional regulator. DIE-1 is present in the nuclei of hypodermal, muscle, gut, and pharyngeal cells; its distribution suggests that DIE-1 acts in each of these tissues to regulate morphogenetic movements. *die-1(w34)* mutants display morphogenetic defects in the pharynx, gut, and muscle quadrants, in addition to the defects in the dorsal hypodermis, consistent with the DIE-1 expression pattern. Mosaic analysis indicates that DIE-1 is autonomously required in the posterior dorsal hypodermis for intercalation. Our analysis documents for the first time the dynamics of protrusive activity during epithelial cell rearrangement. Moreover, our analysis of *die-1* shows that the events of epithelial cell rearrangement are under transcriptional control, and that early and later phases of epithelial cell rearrangement are genetically distinguishable.

INTRODUCTION

Cell rearrangements are known to play a critical role during morphogenesis in both vertebrate and invertebrate systems. There are two main cell types that undergo rearrangement: deep (nonepithelial) cells and epithelial cells. Intercalation of deep cells occurs during epiboly of the animal cap (Keller, 1980; Warga and Kimmel, 1990) and during convergent extension of presumptive axial mesoderm in *Xenopus* and zebrafish (Keller and Tibbetts, 1989; Wilson and Keller, 1991; Warga and Kimmel 1990), and neural tissue in *Xenopus* (Ellul and Keller, 2000). Similarly, in *Drosophila* terminal filament formation involves rearrangement of mesenchymal cells (Godt and Laski, 1995). Several molecular pathways have been implicated in deep

[1] Present address: W.M. Keck Dynamic Image Analysis Facility, Department of Biological Sciences, University of Iowa, City, IA 52242.

[2] Present address: Center for Neurobiology and Behavior, Columbia University, 1051 Riverside Drive, New York, NY 10032.

[3] Present address: Department of Genetics and Developmental Biology, University of Connecticut, 263 Farmington Ave., Farmington, CT 06030.

[4] Present address: Exelixis Pharmaceuticals, Inc., 170 Harbor Way, P.O. Box 511, South San Francisco, CA 94083-0511.

[5] Present address: Department of MCD Biology, Biological Sciences II, University of California, Santa Barbara, CA 93106.

[6] To whom correspondence should be addressed at University of Wisconsin–Madison, Department of Zoology, 1117 W. Johnson Street, Madison, WI 53706. Fax: (608) 262-7319. E-mail: jdhardin@facstaff.wisc.edu.

0012-1606/01 $35.00

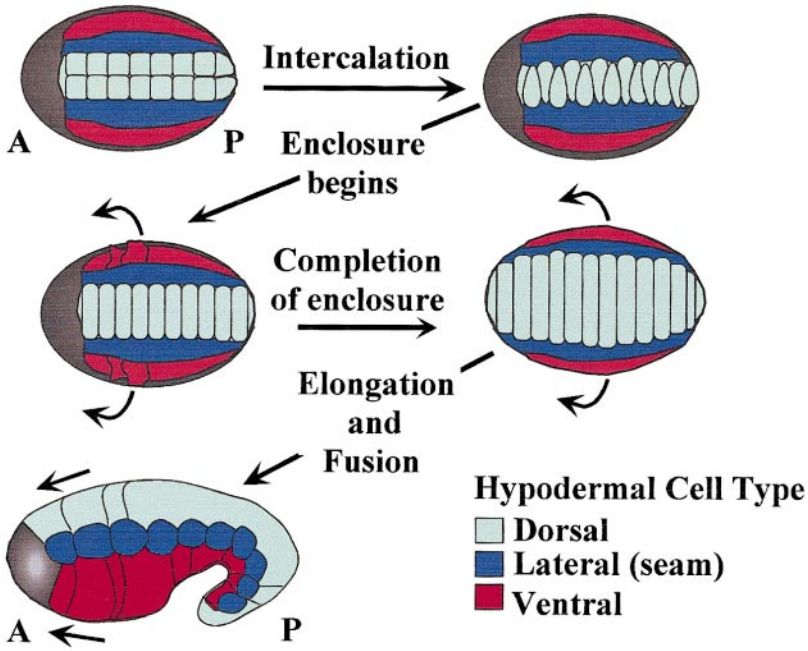

FIG. 1. Schematic diagram of hypodermal morphogenesis in *C. elegans*. Images are intended to portray only relative location, movements, and sequence of morphogenetic events occurring within the hypodermis. For clarity, cell borders have been omitted in the lateral and ventral hypodermis. All diagrams represent dorsal views of unenclosed embryos with the exception of the bottom cartoon, which represents a lateral view of an enclosed and partially elongated embryo. Anterior is to the left in all images. The hypodermis arises as a patch of cells on the dorsal/posterior surface of the embryo; the cells organize into six rows. Intercalation involves the rearrangement of the two central (green) rows of cells into a single row. As intercalation nears completion, enclosure begins with the movement of the outer (red) rows of cells to the ventral midline, followed by anterior spreading of the hypodermal sheet to cover the anterior end of the embryo. This is followed by elongation of the embryo into a wormlike shape. Many of the dorsal and ventral hypodermal cells later fuse into syncytia.

cell rearrangement. The transcription factor BRIC-A-BRAC, a BTB domain transcription factor, is necessary for terminal filament morphogenesis in *Drosophila* ovaries (Godt and Laski, 1995). Likewise, *spadetail,* which encodes a T-box transcription factor, is required for convergence movements of ventrolateral deep cells toward the dorsal side of the embryo in zebrafish (Griffin *et al.*, 1998). Paraxial protocadherin (*papc)* family members also appear to be required in subsets of deep mesodermal cells for proper dorsal convergence movements (Kim *et al.*, 1998; Yamamoto *et al.*, 1998); *papc* has been implicated as a proximal downstream target of *spadetail,* suggesting that *spadetail* may regulate expression of genes directly involved in cell rearrangement. Recently, it was shown that *Wnt-11* and *disheveled* family members mediate planar polarity signals in both zebrafish (Heisenberg *et al.*, 2000) and *Xenopus* (Tada and Smith, 2000; Wallingford *et al.*, 2000) that are required for proper convergence of paraxial mesoderm toward the dorsal midline.

In contrast, less is known about epithelial cell rearrangement, despite its widespread occurrence. Examples include movements at the margin of the enveloping layer in teleosts (Keller and Trinkaus, 1987), shaping of the neural plate in avian embryos (Schoenwolf and Alvarez, 1989), elongation of the archenteron during sea urchin gastrulation (Ettensohn, 1985; Hardin, 1989), intercalation of intestinal cells in *C. elegans* (Leung *et al.*, 1999), germband extension (Irvine and Wieschaus, 1994), and posterior spiracle development (Brown and Castelli-Gair Hombría, 2000) in *Drosophila.* The mechanisms that regulate cell rearrangement in epithelia are unclear. Gap genes appear to be at least indirectly required for coordination of germ band extension movements in *Drosophila* (Irvine and Wieschaus, 1994), although it is not known at what level they exert their influence. In the posterior spiracles, the GATAc protein encoded by *grain* is required for the rearrangement of cells in the stigmaphore (Brown and Castelli-Gair Hombría, 2000); what cell behaviors or processes GATAc regulates are unknown.

The simplicity of the embryonic hypodermis, or epidermis, of the nematode *Caenorhabditis elegans* makes it a convenient system in which to study epithelial cell rearrangement, because individual epithelial cells can be unambiguously identified from embryo to embryo. The hypodermis forms as a patch of 78 cells on the dorsal and lateral surfaces of the posterior region of the embryo. The first morphogenetic movement within this tissue involves the intercalation of 20 cells along the dorsal midline that eventually form the dorsal hypodermis (Williams-Masson *et al.*, 1998). Specific cell migrations within the future ventral hypodermis begin as the process of intercalation is completing, and these movements are necessary for the process of enclosure (Williams-Masson *et*

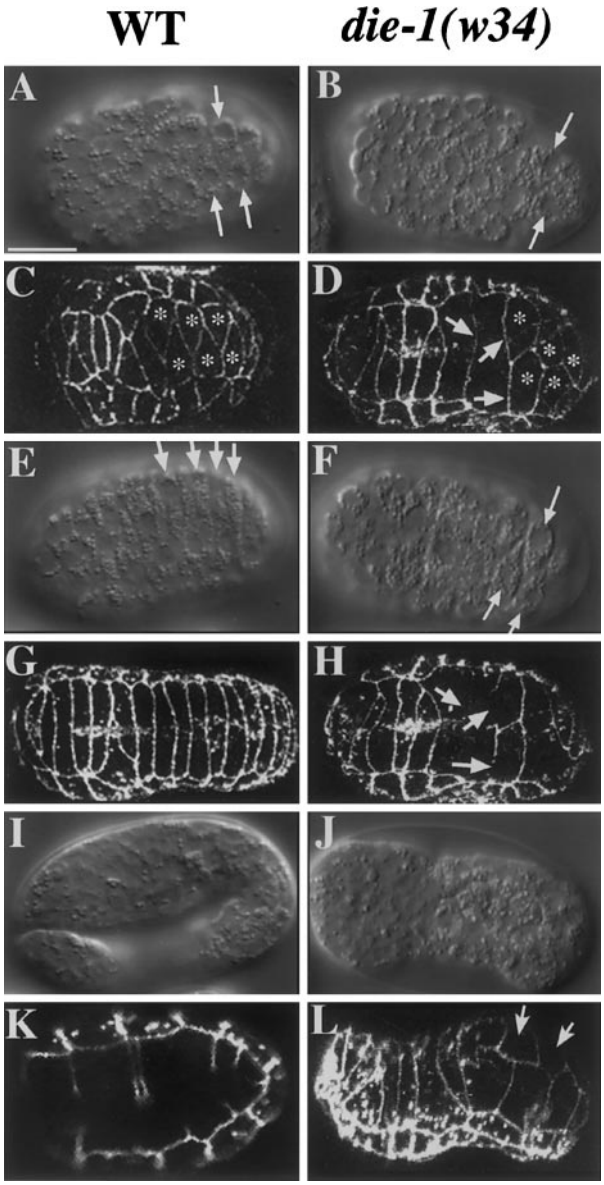

FIG. 2. Intercalation is defective in homozygous *die-1(w34)* embryos. Wild-type ((left column) and *die-1(w34)* mutant (right column) embryos at various stages of morphogenesis. Alternating pairs of figures are Nomarski and multiphoton laser scanning microscopy views of different, but comparably staged, embryos. Embryos in this and all figures are presented with anterior to the left. (A, B) Wild-type and *die-1(w34)* embryos shortly after all hypodermal cells have formed. Arrows indicate dorsal cells that have become wedge shaped (A, B). (C) Wild-type embryo 35 min after the onset of *JAM-1::GFP* expression. Intercalation has just begun. Dorsal posterior hypodermal cells marked with asterisks have wedged between one another. (D) *die-1(w34)* embryo 65 min after the onset of *JAM-1::GFP* expression. Many of the anterior dorsal hypodermal cells have intercalated; however, most of the posterior dorsal cells are wedged and have not completed intercalation (asterisks). Arrows indicate cell boundaries that will fuse prematurely (see H). (E) Same embryo as A, 60 min later. Intercalation is essentially complete. Arrows indicate dorsal cells that have become narrower along the anterior/posterior (A/P) axis, elongated along the left/right (L/R) axis, and have finished intercalation. (F) Same embryo as B, 120 min later. Arrows indicate cells that fail to complete intercalation. Wedged tips have not moved to make contact with the opposing lateral hypodermal cells. Cells have extended along the L/R axis but have not become significantly narrower in the A/P axis. (G) Completely intercalated dorsal hypodermis in a wild-type embryo 100 min after the onset of *JAM-1::GFP* expression. (H) Same embryo as in B, 80 min after the onset of *JAM-1::GFP* expression. Arrows indicate cell boundaries that have started to fuse. (I) Same embryo as in A, 200 min later, lateral view. The embryo has elongated to twice its original length. (J) Same embryo as B, 200 min later. Elongation has failed. (K) *JAM-1::GFP* expression in an *eff-1(oj55)* embryo comparable to I. Elongation is normal. (L) Reconstruction of *JAM-1::GFP* expression in a terminal *die-1(w34); eff-1(oj55)* embryo; for clarity, the gut and intestinal expression has been omitted by "coring" the embryo as in Mohler and White (1998). Unintercalated cells in the posterior are clearly visible (arrows). Siblings had fully elongated. Scale bar = 10 μm.

al., 1997). Enclosure is followed by the elongation of the embryo into a wormlike shape (Priess and Hirsh, 1986). Once enclosure is complete and elongation is under way, many cells of the dorsal and ventral hypodermis fuse into large multinucleate syncytia (Podbilewicz and White, 1994; Mohler *et al.,* 1998). The major events of epithelial morphogenesis in *C. elegans* are summarized in Fig. 1.

Previous studies of dorsal intercalation in *C. elegans* showed that dorsal hypodermal cells are initially organized in two rows on the dorsal surface of the embryo (Sulston *et al.,* 1983; Williams-Masson *et al.,* 1998). Cells within each dorsal row rearrange by extending wedge-shaped protrusions between cells in the contralateral dorsal row; the cell tips then migrate until they meet the opposing row of lateral hypodermal cells. The end result of these movements is the formation of a single row of 20 dorsal hypodermal cells. Treatment of wild-type embryos with nocodazole or cytochalasin D prevents intercalation (Williams-Masson *et al.,* 1998), suggesting that intercalation is dependent on both actin filaments and microtubules.

To determine what role dorsal intercalation plays in the subsequent morphogenesis of the organism and to understand how intercalation movements are regulated at the molecular level, we have undertaken a genetic analysis of the process. In this investigation we analyze *die-1* (*d*orsal *i*ntercalation and *e*longation defective), a gene required for cell rearrangement in the dorsal hypodermis of *C. elegans.* We show that the posterior dorsal hypodermal cells of *die-1* mutant embryos initiate, but cannot complete, intercalation. We also show that mutant embryos enclose with hypodermis but fail to elongate. *die-1* encodes a putative zinc finger protein expressed in cells that display abnormal morphogenesis in the mutant. Mosaic analysis indicates that DIE-1 is specifically required in dorsal hypodermal cells for intercalation to occur. Our results indicate that DIE-1 regulates directed epithelial cell rearrangement in *C. elegans.*

MATERIALS AND METHODS

C. elegans Strains

The Bristol strain N2 was used as wild-type (Brenner, 1974). Nematodes were grown at 20°C in all experiments and were cultured as described by Brenner (1974). To map and balance *die-1*, the following mutations and deficiencies were obtained from the *C. elegans* Genetic Stock Center: LG I, *bli-4(e937)*; LG II, *rol-6(e187), unc-4(e120), let-23(mn23), let-31(mn31), let-242(mn90), let-243(mn226), let-244(mn97), let-268(mn189), vab-9(e1744), mnC1, mnDf12, mnDf14, mnDf28, mnDf61, mnDf62, mnDf63, mnDf66, mnDf68, mnDf71, mnDf83, mnDf89*; LG III, *vab-7(e1562)*; LG IV, *unc-31(e928), him-8(e1489)*; LG V, *dpy-11(e224), him-5(e1467). wDf5* (linkage group II) was isolated in a screen for zygotic lethal mutations (Ferguson *et al.*, 1996; our unpublished data). For additional phenotypic analysis of *die-1(w34), eff-1(oj55),* LG II, *jcIs1 (jam-1::gfp),* linkage group IV (Mohler *et al.*, 1998), and *ojEx3* were used. *jcIs1* is an integrated version of *jam-1::gfp,* and was crossed into the *die-1* background by standard genetic techniques. The *eff-1* mutant is zygotic recessive viable, and lacks cell fusion during embryogenesis (W. A. Mohler, unpublished observations). Heterozygous *die-1(w34)* males were mated into homozygous *eff-1(oj55); jcIs1* hermaphrodites. To generate double mutants, recombinants were identified by singling *eff-1* homozygous F2 progeny; subsequent matings were performed to obtain *eff-1; jcIs1; die-1/+* hermaphrodites. *ojEx3* was produced by injection of plasmid pKK1, which carries a GFP transcriptional reporter for the *lbp-1* gene (Plenefisch *et al.*, 2000). This reporter is expressed at high levels in dorsal hypodermal cells.

Genetics

die-1(w34) was isolated from a general, genome-wide screen for ethylmethane sulfonate (EMS)-induced zygotic embryonic lethal mutations (for methods see Ferguson *et al.*, 1996). *die-1(w34)* was mapped to linkage group II by standard techniques. Recombination between *rol-6* and *unc-4* placed *die-1* very near or to the right of *unc-4*. Complementation tests against deletion mutants placed *die-1* between *egl-43* and *daf-19*.

Rescue

die-1(w34) was mapped to linkage group II between *egl-43* and *daf-19*, a 0.2 map unit interval corresponding to ~300 kb of DNA. *die-1(w34)* fails to complement the deficiency *mnDf71* and complements deficiencies *mnDf61* and *mnDf83*, as well as the lethal mutations *let-242(mn90), let-243(mn226),* and *let-244(mn97).* Cosmids spanning the region between *egl-43* and *daf-19* were obtained from the *C. elegans* Genome Consortium and were tested for transformation rescue by coinjection with the dominant marker *rol-6(su1006)* (Mello *et al.*, 1991). One pool of three clones that rescued *die-1* to viability was identified, and subsequently the injection of a 10-kb subclone of cosmid K10A2 was shown to be sufficient for rescue.

The cDNA yk83h8, obtained from the *C. elegans* cDNA Project (Y. Kohara), was the longest cDNA that mapped to the minimal *die-1* rescuing genomic fragment. yk83h8 was sequenced using ABI PRISM dye terminator cycle sequencing (Perkin Elmer Cetus Instruments, Norwalk, CT). Genomic sequence from cosmid C18D1, available from the *C. elegans* Genome Consortium, agrees with our cDNA sequence and indicates that the *die-1* locus consists of six exons included in the 10-kb rescuing fragment.

The genomic region of the *die-1* locus was amplified from homozygous *die-1(w34)* embryos by the single-embryo PCR method (Williams *et al.*, 1992). The following sets of primers were used to amplify the genomic region in three fragments that span the predicted coding sequence: GGTGGAAGATTACAAGGAGGATACGGAC, ATCAGGAGCCAGAAGAACAACGAG; AGTCTATCCCTTCTCCCTTCAC, TCTGCTTCTGATTCTGCTGATG; and TTTTCGGTTCTTTCTTAGTATTTCG, GAAAAAAGTAGACCTACAAATGGC. In some cases nested internal primers were used to obtain single amplification products. All PCR products were subcloned into either pT7 vector (Novagen, Madison, WI) or PCR-Script (Stratagene, La Jolla, CA). For each amplification product three subclones of two independent samples were sequenced.

Phenotypic Analysis and Live Fluorescence Microscopy

Phenotypic analysis and image acquisition of Nomarski images were performed as previously described (Raich *et al.*, 1998), with the following modifications: 15–24 optical sections of live embryos were recorded every 30–60 s. To monitor GFP expression using *jcIs1* and *ojEx3* in living embryos, mounted embryos were filmed using multiphoton laser scanning microscopy (MPLSM). Data acquisition and stereo-4D processing were performed as previously described (Raich *et al.*, 1999). In brief, Bio-Rad PIC format files were imported into NIH Image using customized Stereo-4D Macros (Mohler and White, 1998). Postimage processing was conducted on a Power Macintosh G3. Time-point projection stacks were converted in 4D Turnaround and 4D Viewer into appended 4D QuickTime movies and replayed as stereo-4D animations using a modified version of NIH Image. All macros, the standard version of NIH Image, and 4D Turnaround/Viewer are available at http://www.bocklabs.wisc.edu/imr/stero4d/stereo4d.html. The modified version of NIH Image is available from J. Hardin.

Antibody Production and Immunostaining

Rabbit polyclonal antibodies recognizing DIE-1 were raised and affinity-purified against the following peptide: ALNLTFKNDGTKKEIEE (Quality Controlled Biochemicals, Hopkinton, MA). A modified version of the freeze-crack method (Miller and Shakes, 1995) was used to process embryos for immunostaining essentially as previously described (Raich *et al.*, 1998). Affinity-purified DIE-1 antiserum and GFP antiserum (Novagen) were added at 1:200 dilution, monoclonal MH27 antibody (kindly provided by Robert Waterston) was added at a 1:500 dilution, and the monoclonal body muscle antibody NE8/4C6.3 (Goh and Bogaert, 1991) was added at a 1:20 dilution. All primary antibodies were diluted into a solution of nonfat dry milk and applied to fixed specimens for 1 h at 37°C. The samples were washed twice in PBST for 5 min and incubated in FITC (Sigma Chemical Co., St. Louis, MO) or Texas Red-conjugated secondary antibodies (Jackson ImmunoResearch, West Grove, PA) diluted 1:100 in PBST + 0.5% nonfat dry milk for 1 h at 37°C. The specimens were rinsed in PBST buffer and sealed in a drop of Slowfade antibleaching solution (Molecular Probes, Eugene, OR).

To analyze the organization of actin filaments within the hypodermis of *die-1(w34)* mutants, embryos were collected and stained with phalloidin as previously described (Costa *et al.*, 1997). The only modification to this protocol was the use of Alexa 488 phalloidin (Molecular Probes) at a concentration of 10 units/ml. Fluorescent images of fixed samples were obtained using a Bio-Rad MRC1024 confocal laser scanning microscope.

die-1::gfp Translational Fusion

A minimal *die-1* rescuing fragment was linearized by digestion with *Mlu*I, which cuts uniquely in the first intron of *die-1*. The GFP intron insertion vector pPD103.75 (courtesy of A. Fire, Carnegie Institution of Washington) was also cut with *Mlu*I, which drops out a fragment containing the entire GFP sequence flanked by consensus sequences for intron donor and acceptor splice sites. This fragment was cloned into the linearized *die-1* rescuing vector. This construct was co-injected into *die-1/mnC1* animals with *jam-1::gfp* and pRF4 (*rol-6*). A strain carrying an extrachromosomal array of these constructs (*jcEx23)* can rescue *die-1(w34)* homozygous embryos to viability, showing that DIE-1 remains functional with GFP inserted near its amino terminus. This array was subsequently integrated into the genome by crossing it into an N2 background, treating animals with 3000 rad of γ-irradiation, and identifying animals that produce 100% rollers in the F2 generation (Mello and Fire, 1995). GFP expression was visualized in living embryos using standard epifluorescence and MPLSM. Expression was weakly detected in some nuclei but could not be seen consistently or clearly. To enhance the GFP signal, embryos were processed via the freeze-crack method, stained with rabbit polyclonal anti-GFP antibodies (Novagen), and processed for immunofluorescence as described earlier.

Mosaic Analysis

To assess the role of DIE-1 in specific cells, animals expressing *die-1::gfp* in mosaic fashion were identified and analyzed for proper intercalation. Embryos from the rescued strain carrying *jcEx23* were fixed and stained with GFP polyclonal antiserum followed by FITC-conjugated goat anti-rabbit secondary antibody and at the same time stained with monoclonal MH27 antibody followed by Texas Red-conjugated goat anti-mouse secondary antibody. This allowed visualization of all epithelial cell boundaries in the red channel; epithelial junctions could also be seen in the green channel in those cells that expressed the array. Mosaics were identified as embryos lacking epithelial staining in some cells in the green channel (see Results). Mosaic embryos were subsequently analyzed for morphogenetic defects.

Northern Blot

To determine the number and sizes of transcripts produced from the *die-1* locus, total RNA was prepared from wild-type worms as previously described (Burdine *et al.*, 1997). Poly(A)$^+$ RNA was then isolated using the PolyATtract kit (Promega Corporation, Madison, WI). RNA (2 μg per lane) was loaded on a 1.2% agarose (w/v), 16% formamide (v/v) gel. The gel was blotted onto Hybond-N+ nylon filter (Amersham, Buckinghamshire, UK) and RNA was cross-linked to the filter using a UV-Stratalinker 1800 (Stratagene) for 30 s. The probe was generated from linearized *die-1* cDNA that was gel-purified using the Qiaquick Gel Extraction kit (Qiagen, Santa Clarita, CA). A 100-ng sample of purified cDNA was labeled using random decamers, 1 μl Klenow, 5 μl dCTP^{32}, and 2.5 μl of a mix that contained dA, dT, and dG at 1 mM each. The reaction was incubated for 1 h at room temperature. The Northern blot was prehybridized for 30 min at 65°C in Denhardt's reagent (Sambrook *et al.*, 1989). The probe was purified by passage over a spin column and hybridizations were performed at 65°C for 24 h. Blots were washed three times for 30 min in 0.1× SSPE and exposed to Scientific Imaging Film (Kodak, Rochester, NY).

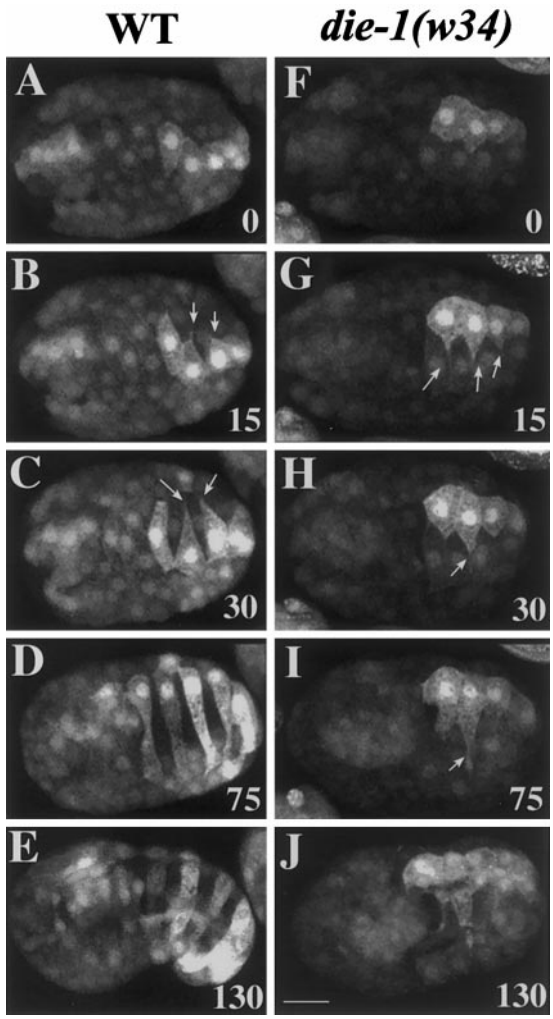

FIG. 3. Analysis of protrusive activity in dorsal hypodermal cells in *die-1(w34)* embryos. Wild-type (left, A–E) and *die-1(w34)* (right, F–J) embryos carrying a *lbp-1::gfp* transcriptional reporter (Plenefisch *et al.*, 2000) were analyzed using multiphoton microscopy. Times (in min) are indicated in the lower right corner of each frame; in each case, filming commenced within 5–10 min of completion of the terminal divisions of the C-derived dorsal hypodermal cells. To suppress cell fusion, both strains were made homozygous for the *eff-1(oj55)* allele. Small arrows indicate basolateral protrusions extended by the dorsal hypodermal cells. In *die-1(w34)* embryos, protrusions are extended (G–I), although cell translocation does not occur (J). Scale bar = 10 μm.

RESULTS

die-1 Is Required for Rearrangement of Dorsal Hypodermal Cells and Elongation of the Embryo

The first observable defect in *die-1(w34)* homozygous embryos is the failure of posterior dorsal hypodermal cells to undergo intercalation (Fig. 2). *die-1(w34)* embryos produce the normal complement of hypodermal cells and the dorsal cells become wedge-shaped as in wild-type embryos

(Fig. 2B). However, posterior dorsal cells fail to finish the process of intercalation and remain wedge-shaped until they eventually fuse into syncytia (Fig. 2D). Despite abnormal intercalation, *die-1(w34)* embryos still enclose with hypodermis (Fig. 2F). Significantly, the process of elongation is also affected in *die-1(w34)* embryos. Wild-type embryos elongate to almost four times their initial length; *die-1(w34)* embryos never elongate more than twice their initial length (Figs. 2I–2L).

To visualize hypodermal boundaries more clearly, a *jam-1::gfp* translational fusion construct was expressed in *die-1(w34)* homozygous embryos. *JAM-1::GFP* is expressed at the junctional borders of all epithelial cells in *C. elegans,* allowing the analysis of hypodermal cell movements in developing *die-1*(*w34)* embryos with the use of multiphoton laser scanning microscopy (MPLSM) (Mohler *et al.,* 1998; Raich *et al.,* 1999). Anterior dorsal hypodermal cells derived from the AB founder cell successfully intercalate in mutant embryos (Fig. 2). In contrast, intercalation defects are readily apparent in posterior dorsal hypodermal cells in *jam-1::gfp*-expressing *die-1(w34)* embryos (Fig. 2D). The posterior dorsal hypodermis is derived from the C founder cell (Sulston *et al.,* 1983; Williams-Masson *et al.,* 1998). Based on the position of unintercalated cells in *die-1(w34)* mutants, the anteriormost pair of C-derived cells consistently intercalate. In 12 out of 12 multiphoton movies in which dorsal hypodermal cells could be unambiguously identified, this pair of cells completed intercalation. In contrast, the remainder of the C-derived dorsal hypodermal cells displays intercalation failure. The posterior C-derived dorsal hypodermis was never observed to progress beyond wedging, consistent with results obtained via anti-JAM-1 immunostaining using the MH27 antibody (data not shown).

TABLE 1
Timing of Cell Fusion and Enclosure

	Time to first fusion[a] (min ± SEM)[d]	Time to last fusion[b] (min ± SEM)	Time to enclosure[c] (min ± SEM)
wild-type	121 ± 4.2 (n = 4)	167 ± 16.9 (n = 3)	74 ± 2.3 (n = 8)
die-1(w34)[e]	75 ± 5.8 (n = 3)	133 ± 6.0 (n = 3)	73 ± 2.4 (n = 3)

[a] Time to first fusion was defined as the first time point at which a cell appeared completely or partially fused in the dorsal hypodermis.
[b] Time to last fusion is the first time point at which all dorsal hypodermal cells appeared fused.
[c] Time to enclosure is defined as the first time point at which the leading cells of the ventral hypodermis have clearly met at the ventral midline.
[d] min = time from initial expression of JAM-1::GFP to described phenomenon.
[e] Homozygous mutant embryos from heterozygous *die-1(w34)* animals expressing *jam-1::gfp* were analyzed.

Late Steps in Intercalation Are Defective in die-1(w34) Embryos

Previous studies of fixed material indicated that intercalating dorsal hypodermal cells extend basolateral protrusions beneath the level of the adherens junction as they begin to interdigitate (Williams-Masson *et al.,* 1998). To examine these protrusions dynamically in living *die-1(w34)* embryos, we used a transcriptional reporter for *lbp-1* (Plenefisch *et al.,* 2000) to drive expression of GFP in posterior dorsal hypodermal cells during intercalation. In addition, we used *eff-1(oj55)* to suppress cell fusion so that the position of individual dorsal cells could be scored in terminal embryos. *eff-1(oj55)* mutants are homozygous viable, undergo dorsal intercalation normally, and are normal in other respects, but lack cell fusion during embryogenesis (W. A. Mohler, unpublished observations). Within 10 min following the terminal divisions of the dorsal hypodermal precursors, dorsal hypodermal cells in wild-type embryos extend protrusions toward the dorsal midline in the direction in which their cell bodies ultimately translocate (Figs. 3A–3E). Initially, pulsatile activity is detectable on both the medial and lateral edges of cells (Fig. 3A). Shortly after protrusive activity is detectable the preponderance of protrusive activity becomes confined to the medial tips of the cells (Figs. 3B and 3C). There is little deviation of these protrusions along the anterior–posterior axis, that is, the protrusions are extended in a highly directional manner from right to left or left to right. In wild-type embryos, the lateral region of the cell undergoes a change in shape following the extension of a medial protrusion (Fig. 3C), such that the entire cell begins to elongate mediolaterally toward the contralateral side of the embryo until it spans the entire width of the dorsal hypodermis (Fig. 3D). The dynamic analysis of dorsal intercalation shows that (1) intercalating cells are polarized along the right-left (i.e., mediolateral) axis very rapidly after they are born, (2) intercalating cells are protrusively active throughout intercalation, and (3) protrusion extension is rapidly consolidated into a corresponding change in the shape of intercalating cells.

MPLSM analysis of *die-1(w34);eff-1(oj55)* embryos indicates that C-derived dorsal cells appear normal during the early phase of intercalation. C-derived dorsal cells extend dynamic protrusions that appear indistinguishable from those in wild-type embryos and appear correctly polarized by the time the cells' apical surfaces become wedge-shaped [n = 6 embryos examined for both *eff-1(oj55)* and *die-1(w34);eff-1(oj55);* Figs. 3A, 3B, 3F, and 3G]. However, the cell bodies of C-derived posterior dorsal cells fail to translocate (Figs. 3H and 3I). These results indicate that C-derived dorsal hypodermal cells are polarized in *die-1(w34)* embryos and that they can extend protrusions that are normally associated with cell rearrangement prior to later defects in cell translocation.

die-1(w34) embryos appear to undergo premature fusion of the dorsal hypodermis, based on timing of fusion relative to the onset of *jam-1::gfp* expression (Fig. 2H). Measure-

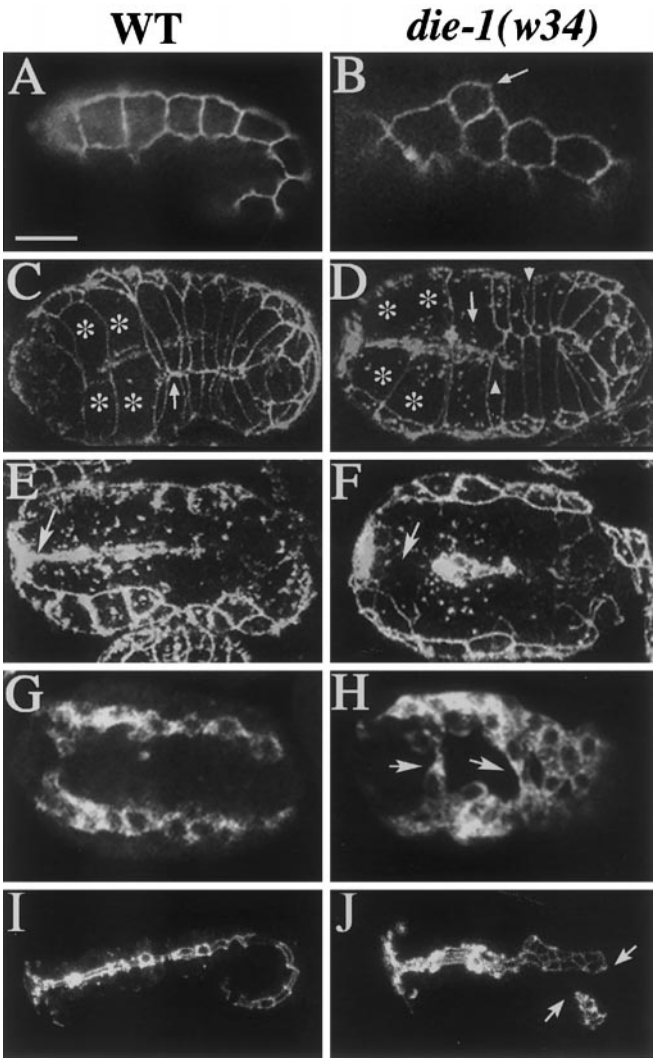

FIG. 4. Additional defects associated with *die-1(w34)* embryos. Wild-type embryos are shown in the left column, *die-1(w34)* embryos on the right. (A, B) Lateral views of wild-type and *die-1(w34)* embryos stained with MH27 antibody. (A) In wild-type embryos, lateral cells form linear rows of 10 cells per side. (B) *die-1(w34)* embryos typically have lateral cells pinched out of the row (arrow). (C, D) Ventral views of wild-type and *die-1(w34)* embryos expressing *JAM-1::GFP,* as viewed with multiphoton microscopy. Both embryos are enclosed with hypodermis and are approximately the same age. Asterisks indicate the same cells in both embryos. (C) Hypodermal cells in a wild-type embryo meet at the ventral midline in a pairwise manner. The arrow indicates a junction at the midline between a specific pair of cells. (D) A *die-1(w34)* embryo; cells have met at the midline out of register. Small arrowheads indicate cells that failed to reach the midline. The arrow indicates the missing junction between the same pair of cells highlighted in C, which have fused prematurely. (E, F) Wild-type (E) and *die-1(w34)* (F) embryos expressing *JAM-1::GFP,* as viewed by multiphoton microscopy. (E) An embryo displaying normal attachment of the pharynx to the buccal cavity (arrow). (F) *die-1(w34)* embryo in which the pharynx has failed to attach to the buccal cavity. Arrow indicates absence of JAM-1-expressing cells between the pharynx and buccal cavity. (G, H) Wild-type (G) and *die-1(w34)* (H) embryos stained with the body wall muscle-specific antibody NE8/4C6.3. (G) Body muscle cells separate into distinct quadrants prior to elongation of the animal. The two dorsal quadrants can be seen in this image. (H) *die-1(w34)* embryos also display four muscle quadrants but often exhibit crossover of tissue between rows (arrows). (I, J) 3D reconstructions of wild-type (I) and embryos derived from a *die-1(w34)* germline mosaic mother (J) stained with MH27. The exterior focal planes have been removed and the focal planes containing the gut have been reconstructed. Arrows in J indicate sites at which the posterior intestine has detached from the anterior intestine (upper arrow) and the anal region (lower arrow). Scale bar = 10 μm.

ments from multiphoton recordings indicate fusion occurs approximately 45 min early in *die-1(w34)* embryos. In contrast, ventral enclosure occurs at the same relative time in both mutant and wild-type embryos (Table 1). Although fusion occurs early in *die-1(w34)* homozygotes, we were able to show that the precocious fusion phenotype does not account for the intercalation defects in *die-1(w34)* mutants by producing *die-1(w34);eff-1(oj55);jam-1::gfp* embryos. Although *eff-1(oj55)* single mutants undergo normal intercalation, we found that intercalation still fails to occur in *die-1(w34);eff-1(oj55)* double-mutant embryos, even though dorsal cells do not fuse (Fig. 2L). The posterior dorsal cells did not intercalate by the time muscle activity was observed (data not shown), more than 2 h after intercalation begins in wild-type embryos. This indicates that the process of intercalation is not simply delayed in *die-1(w34)* embryos and that precocious fusion is not masking dorsal cell rearrangement in *die-1(w34)* mutants.

die-1(w34) Mutant Embryos Display Additional Morphogenetic Defects

We were able to identify other morphogenetic defects within *die-1(w34)* embryos. In wild-type embryos the lateral hypodermis consists of two linear rows of 10 cells, one on each side of the embryo (Fig. 4A). *die-1(w34)* terminal embryos appear to have one or two cells pinched out of each lateral row (n = 30 out of 30 examined via MH27 immunostaining; Fig. 4B). This phenotype was observed only in older embryos, after the intercalation defect was already apparent. The initial pattern of lateral cells appears to be normal in all *die-1(w34)* embryos examined. We also observed defects associated with the ventral hypodermis. In wild-type embryos, ventral cells meet at the midline in a pairwise manner. Most of these pairs of cells form new adherens junctions once they reach the midline, whereas some of the anterior pairs of cells fuse with each other upon contact (Raich *et al.*, 1999). In *die-1(w34)* embryos we frequently observed incorrect cell fusions (5/6 embryos examined via MPLSM), skewed pairing of cells (5/6 embryos), and failure of some cells to reach the ventral midline (4/6 embryos; see Fig. 4D). Despite the abnormal arrangement of ventral hypodermal cells, mutant embryos consis-

tently enclosed with hypodermis, indicating that intercalation is not a prerequisite for ventral enclosure.

die-1(w34) embryos also display nonhypodermal defects in tissues that are known to undergo rearrangement along the anterior–posterior axis. In wild-type animals, the pharynx develops as a cluster of cells in the anterior half of the animal. The pharynx eventually elongates, connecting to the surface of the embryo via the buccal cavity (Fig. 4E). Nine of 33 *die-1(w34)* embryos analyzed using *jam-1::gfp* were determined to have defects in pharynx attachment (Fig. 4F). To examine body wall muscle, immunostaining experiments were performed with NE8/4C6.3, a body muscle-specific antibody (Goh and Bogaert, 1991). Body muscle cells appeared to be present in normal quantities and were generally organized into four quadrants, as is the case in wild-type. In wild-type embryos, muscle cells organize into tight rows within each quadrant and muscle tissue is never observed to cross between quadrants (Fig. 4G). However, in *die-1(w34)* mutants, crossing between quadrants was observed (Fig. 4H). Crossing of muscle was primarily confined to the posterior half of the embryo. Finally, in wild-type embryos, the intestinal rudiment is attached to the posterior region of the pharynx at its anterior end and the anus at its posterior (Fig. 4I). In contrast, in *die-1(w34)* mutants we observed cases in which the intestine appeared severed from either the posterior pharynx or the anus, or both, resulting in a straight intestine, rather than the typical curved rudiment at the comma stage (n = 11 out of 22 embryos examined; similar results were obtained from the offspring of *die-1(w34)* germline mosaic mothers; Fig. 4J). These results suggest that *die-1* is required for multiple cell rearrangement events within the embryo, in addition to those associated with dorsal intercalation.

Cytoskeletal Arrays Form, but Do Not Organize Properly, within the Dorsal Hypodermis of die-1(w34) Embryos

Actin and microtubule inhibitors (Priess and Hirsh, 1986; Williams-Masson *et al.,* 1998) and loss-of-function mutations in the actin-binding protein α-catenin (Costa *et al.,* 1998; Raich *et al.,* 1999) are known to disrupt elongation in *C. elegans* embryos. To address whether actin organization is disrupted in *die-1(w34)* mutants, we stained embryos from *die-1(w34)* heterozygous hermaphrodites with phalloidin. Actin forms into parallel, circumferentially oriented arrays within the dorsal hypodermis of wild-type animals (Fig. 5A). As elongation proceeds these arrays become uniformly spaced, thicker, and more distinct (Fig. 5B). Constriction of these filaments is thought to result in the subsequent elongation of the embryo (Priess and Hirsh, 1986). In *die-1(w34)* embryos the dorsal midline region of the dorsal hypodermal syncytium is often devoid of organized actin. In contrast, small regions of organized actin can be seen in lateral regions of the dorsal hypodermis (Fig. 6C). Actin organization often appears relatively normal in the anterior dorsal hypodermis of *die-1(w34)* embryos (Fig. 5C). This region corresponds to the region in which intercalation is unaffected in *die-1(w34)* mutant embryos. Terminal *die-1(w34)* mutant embryos display thickened bundles of actin filaments, similar to those in elongating wild-type embryos, but these filaments are discontinuous and nonuniform in appearance (Fig. 5D). Although the defects are less pronounced, we observed similar midline abnormalities in the organization of microtubules in *die-1(w34)* embryos (Figs. 5E and 5F).These data suggest that DIE-1, or the process of intercalation, may be required for cytoskeletal elements to form a continuous, parallel array spanning the dorsal syncytium.

die-1 Encodes a C2H2 Zinc Finger Protein

We mapped *die-1* and determined its molecular identity using standard methods (Figs. 6A and 6B; see Materials and Methods). Comparison of genomic and cDNA sequences revealed that the *die-1* locus consists of six exons (Fig. 6C). The largest cDNA appears to be full length, based on identification of a poly(A) tract at the end of the 3′ UTR, the presence of a Genefinder-predicted start codon, and the presence of stop codons in all three frames of the sequence upstream of the predicted start codon. In addition, the only transcript detected on a Northern blot is 2.9 kb, the size predicted if the cDNA is assumed to be full length (Fig. 6D). Unlike many transcripts in *C. elegans* (Blumenthal, 1995), *die-1* transcripts do not appear to be *trans*-spliced.

die-1 encodes a predicted 645 amino acid protein containing four C2H2 zinc fingers (Fig. 7A). Two hallmarks of C2H2 transcriptional regulators can also be identified (Ptashne, 1988): serine/threonine-rich regions in the amino terminal half of the protein, which are approximately 50% serine or threonine (underlined in Fig. 7A), and two short glutamine-rich regions (amino acids 58–90 and 229–251) upstream of the zinc fingers, in which 7 out of 23 residues are glutamine. All four fingers contain the conserved cysteine and histidine residues associated with C2H2 zinc finger proteins. Three out of four fingers have the conserved leucine residue at position 16, whereas only one of the four fingers has the typically conserved phenlyalanine residue at position 10 (Fig. 7B). Typically, C2H2 zinc finger proteins have a well-conserved 7 amino acid linker region between the individual fingers (Klug and Rhodes, 1987; Schuh *et al.,* 1986). The DIE-1 protein has much longer linker regions. Other examples of long linker regions are known, although their significance is uncertain (Wilson *et al.,* 1994; and unpublished sequences submitted to GenBank). The zinc finger domain is located in the carboxy-terminal half of the protein and there is no significant homology to other proteins outside the zinc finger domain.

We amplified and sequenced the *die-1* region from *die-1(w34)* homozygous embryos. The *die-1(w34)* sequence contains a C to T transition in exon 2 that results in a premature stop codon following amino acid 89 (Fig. 6C). The premature stop codon in *die-1(w34)* truncates the protein prior to the zinc finger domain of DIE-1 and is therefore predicted to destroy its ability to bind DNA. Two

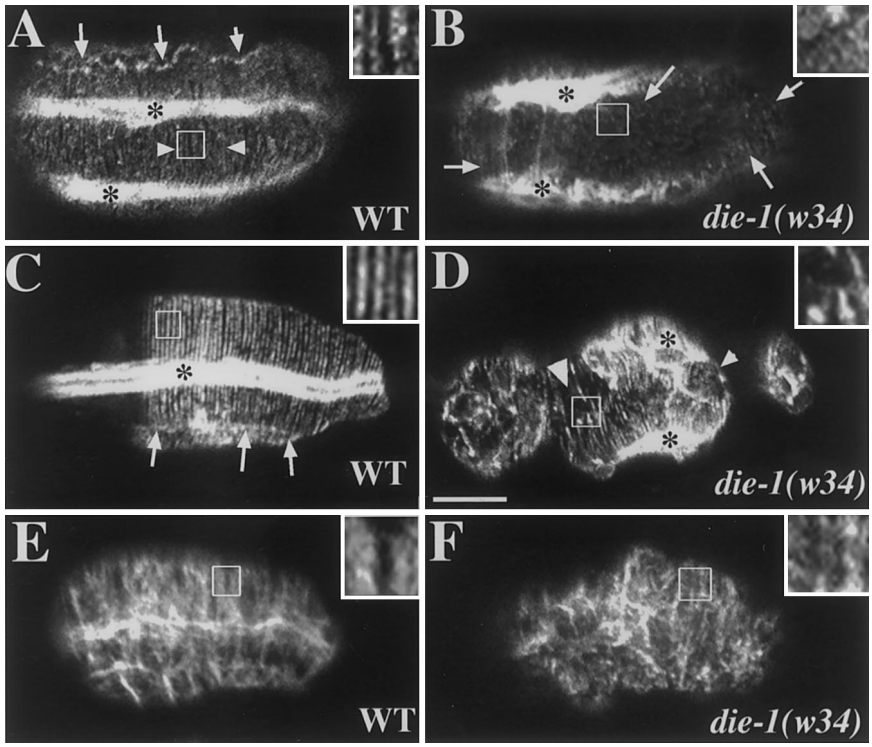

FIG. 5. Actin and microtubule organization in the hypodermis of *die-1(w34)* embryos. Insets are ×3 enlargements of the boxed area in each panel. Intense phalloidin staining running horizontally across the embryo indicates the underlying dorsal muscle in A–D (asterisks). (A) A wild-type embryo shortly after dorsal cells have fused (embryo approximately twofold its original length); dorsal view. Fine actin filaments can be seen within the hypodermis in a mediolaterally oriented pattern (arrowheads). Arrows indicate the boundary between dorsal and lateral hypodermis that runs horizontally across the image. (B) Dorsal view of a *die-1(w34)* embryo shortly after fusion has occurred. This embryo is equivalent in age to the embryo in A. Small regions of organized actin can be discerned (arrows); however, the central region of the dorsal hypodermis does not display organized actin filaments. (C) Dorsal view of a completely elongated wild-type embryo. Actin filaments are thicker and organized into distinct fibrils within the dorsal hypodermis and display uniform spacing. Arrows indicate the boundary between dorsal and lateral cells. (D) Terminal *die-1(w34)* embryos display regions of actin filament organization within the hypodermis; however, filaments often appear discontinuous (arrowheads). (E) Microtubule organization in a wild-type embryo. Partially parallel arrays of microtubules are visible. (F) Microtubule organization in a *die-1(w34)* mutant. Similar arrays are visible. Scale bar = 10 μm.

other lines of evidence suggest that *die-1(w34)* is a null allele: (1) the similarity in phenotype of *die-1(w34)/mnDf71* embryos to that of *die-1(w34)* homozygotes (data not shown) and (2) the phenotypic similarity between *die-1(w34)* homozygotes and *die-1(RNAi)* embryos (data not shown).

DIE-1 Is Expressed in Dorsal Hypodermal Cells prior to and during Intercalation and Also in Other Cells That Display Morphogenetic Defects in die-1(w34) Mutants

We employed two methods to determine when and where DIE-1 protein is expressed during embryonic development. First, we generated anti-DIE-1 polyclonal antibodies. Second, we produced a translational fusion in which *gfp* was inserted in-frame between exons one and two in the smallest rescuing *die-1* clone. *die-1::gfp* rescues *die-1(w34)* embryos to viability, indicating that the fusion protein is functional and expressed in all required cells. Furthermore, DIE-1::GFP faithfully reproduces the wild-type *die-1* expression pattern as determined by immunostaining.

Consistent with its role as a putative transcriptional regulator, DIE-1 is expressed in the nuclei of cells in tissues that display phenotypes in *die-1(w34)* mutants. Maternally expressed DIE-1 can be detected in all blastomeres of the early embryo (data not shown). We infer that such expression represents translation of maternal mRNA based on two pieces of evidence. First, extrachromosomal arrays are not typically well expressed in the *C. elegans* germline (Kelly and Fire, 1998); that *die-1::gfp* is not expressed until the ~50-cell stage suggests that zygotic expression begins at this time. Second, immunostaining of cross-progeny from matings of wild-type males with *die-1(w34)* germline mosaic hermaphrodites indicates that the first detectable expression of zygotic DIE-1 occurs at the ~50-cell stage. Moreover, viable embryos result in either case, which indicates that the early expression of DIE-1 is not required for rescue of all *die-1(w34)* phenotypes. Zygotic DIE-1

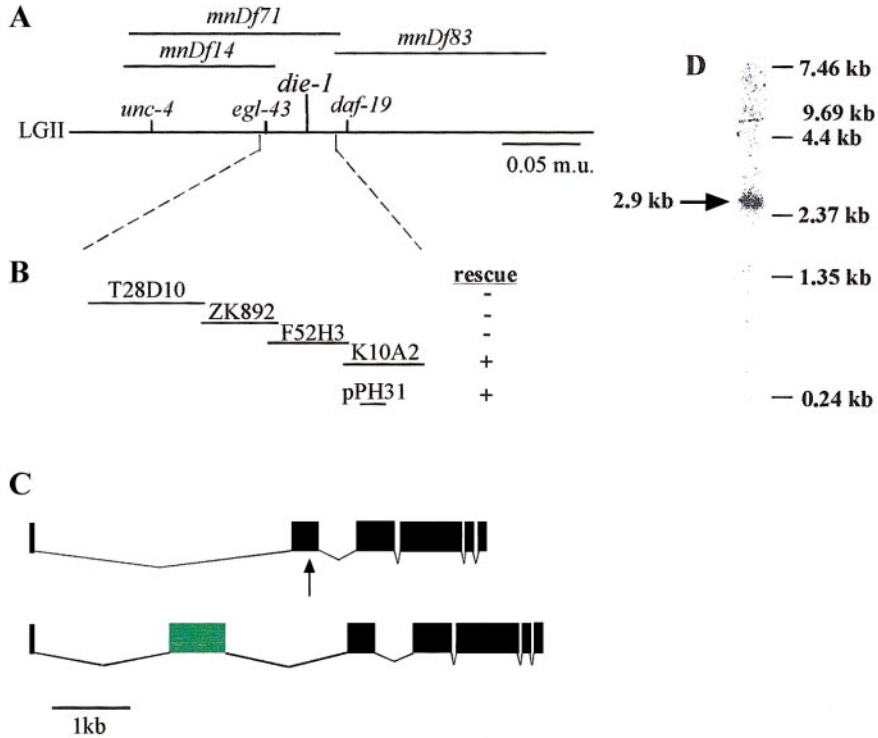

FIG. 6. Mapping and cloning of *die-1*. (A) Genetic map of the region surrounding *die-1*. Three factor-mapping and complementation tests against deletion mutants place *die-1* between *egl-43* and *daf-19*. (B) Cosmids spanning the *die-1* region were injected, and a 10-kb rescuing fragment was isolated (pPH31). (C) Top: intron/exon structure of the only predicted ORF in the smallest rescuing fragment. The arrow indicates the location of a premature stop codon. Bottom: intron/exon structure of the *die-1::gfp* fusion construct generated by insertion of *gfp* coding sequence (represented by gray box) into the first intron of the predicted gene. (D) Northern blot probed with *die-1*-specific probe. A single band was detected at approximately 2.9 kb (arrow).

expression is prominent in the posterior half of the embryo, in the nuclei of muscle and hypodermal precursors (Fig. 8A). When *jam-1::gfp* expression first becomes visible, shortly after the hypodermal cells undergo their terminal divisions, DIE-1 can be detected very strongly in the dorsal hypodermis (Fig. 8B). As intercalation proceeds, DIE-1 expression becomes weaker in these cells. Interestingly, the "pointer" cells, which are the last dorsal hypodermal cells to intercalate (Williams-Masson *et al.*, 1998), maintain elevated levels of DIE-1 longer than other dorsal hypodermal cells. DIE-1 is undetectable in the nuclei of C-derived dorsal cells by the time intercalation is complete (Fig. 8C).

In addition to expression in dorsal hypodermal cells, DIE-1 is present in ventral hypodermal cells during the process of enclosure (Fig. 8D); expression ceases in the hypodermis after enclosure has completed, prior to the process of elongation (see Fig. 8G). The absence of expression during elongation suggests that DIE-1 may not play a direct role in elongation and that the elongation defect is a secondary result of other morphogenetic abnormalities. DIE-1 is also present in pharyngeal cells and in the gut primordium (Figs. 8E and 8F). DIE-1 is also expressed in muscle cells, as confirmed by double-staining *die-1::gfp*-expressing embryos with anti-GFP and muscle-specific antibodies. Nuclei containing GFP indicative of DIE-1 expression were consistently observed within the rows of muscle (Fig. 8G). After enclosure is complete, DIE-1 expression completely disappears in all tissues until late in embryogenesis (Fig. 8H), at which time ~15 cells between the anterior and posterior bulbs of the pharynx express *die-1::gfp* (data not shown). DIE-1 is also present in numerous cells along the ventral midline in L2–L4 larvae (data not shown).

Mosaic Analysis Suggests That DIE-1 Acts within the C Lineage to Promote Intercalation of Posterior Dorsal Hypodermis

To determine whether DIE-1 acts in the C-derived dorsal hypodermis in a cell-autonomous or cell-nonautonomous fashion, we employed two methods. First, we asked whether intercalation movements might be dependent on the presence of underlying C-derived muscle cells in the posterior by ablating Cap and Cpp in wild-type animals. These ablations eliminate 32 of the 81 body muscle cells present at the end of embryogenesis and approximately half of the dorsal muscle cells that are present in the two quadrants that underlie the dorsal hypodermis. Three embryos were ablated and intercalation was observed to pro-

A

```
MANAVDMQQL LMSMDPSSAN QFNMMNKGGA CVMATSGGSA SPTSSSGAPS   50
SSSIMAETDE KDMFMPSQLI QNGLANNQLM SMILQQQSNQ ADSNIADAGH  100
NNSGAEKNII ELLMSGNADL MKFATQFAQQ AKSVDQEPEE QRESSPSPPP  150
AVSLNSTLAS MVFPTTSTAT ECSAASTTSS VDSAPSTVIV NGHSNSQSNT  200
DDDDVTQQPS AKKQRTGDET PLTPTSNNQL MQSLLAQMGL SNPLHQQNQK  250
QMKDESMMFS GLFPQGLAGI PLMFQSPLHQ QFAGMQDFEP LSALSTPNKG  300
SGVKRQYSSN NKNFCDICNK EVCNKYFLRT HMLKMHGIVI DENKTVIANI  350
DTSIKEREGE LTFRCDTCRT MFKTRNQLRQ HRQDVHGVLP LSTPRNNPNK  400
SSVPTTPNGA NNNSGPNSAS MSEEKCALCD KRVSPSMMML HMAQDHFGAA  450
AANGDLNQMM AILGQRNQST EEKMSSNLLE CTDCSYKTRD PKNLDLHMER  500
HIKMSEAKGR GDEDEDVALQ LTTEAALQMV VQNQNQYDGD STAAALNLTF  550
KNDGTKKEIE EEKATGNHER NSHTSGSISP SGSIPEGFGK NIGEKAFPTQ  600
SFLIKCNDDS GEFLTEFLAQ LPVRSVIDGP RQLVFNLHPA PPTTS       645
```

B

```
Consensus C--C---F-----L--H----·H
Finger 1  CDICNKEVCNKYFLRTHMLKMH
Finger 2  CDTCRTMFKTRNQLRQHRQDVH
Finger 3  CALCDKRVSPSMMML·HMAQDH
Finger 4  CTDCSYKTRDPKNLDLHMER·H
```

FIG. 7. *die-1* encodes a zinc finger protein. (A) Predicted amino acid sequence of DIE-1. The protein contains four well-conserved C2H2 zinc fingers (underlined), as well as two serine/threonine-rich regions (boxes). These regions were 50% S and T. An asterisk denotes the position of a premature stop codon in *die-1(w34),* which truncates the protein to 89 amino acids. (B) Alignment of the four zinc fingers detected in *die-1* with the consensus sequence for C2H2 zinc fingers. Conserved residues are bold.

ceed normally in each case (Figs. 9A–9C). These results suggest that intercalation occurs independently of the underlying muscle tissue.

Second, we used a *die-1(w34)* homozygous strain containing the rescuing *die-1::gfp* and *jam-1::gfp* in an extrachromosomal array (*jcEx23)* for mosaic analysis. We identified cells that lacked the array by scoring for the loss of *jam-1::gfp* expression; we monitored the shape and position of epithelial cells in such mosaic animals via anti-JAM-1 immunostaining using the MH27 antibody. Given that the dorsal hypodermal defects in *die-1(w34)* mutant embryos are confined to the posterior, we focused on identifying rare losses in the C lineage. Because our ablation results indicated that C-derived dorsal muscle is dispensable for dorsal intercalation, losses in C-derived hypodermis should provide information about DIE-1 requirements in posterior dorsal hypodermal cells. We were able to identify two embryos in which expression of the array was lost from the C lineage, and one in which the array was lost from its precursor P2. In all of these embryos, intercalation defects were apparent in C-derived posterior dorsal cells, with the exception of the anteriormost pair of C-derived hypodermal cells (Fig. 9D). The phenotype of these embryos is consistent with a requirement for DIE-1 function within individual intercalating cells in the posterior.

In contrast, DIE-1 does not appear to be required in ventral hypodermal cells. We identified 11 mosaic embryos with losses in lineages derived from ABp, which generates ventral hypodermal cells, among other cell types. All of these embryos appeared to elongate normally (Fig. 9E), suggesting that DIE-1 function within the ABp lineage is not critical for morphogenesis of the embryo. As an additional by-product of this analysis, other mosaic losses in epithelial cells were identified. In two embryos complex mosaic losses were sustained in cells that generate the gut (one in EMS, another in E), as well as cells in AB lineages; both exhibited misshapen guts with an abnormally wide lumen and abnormal organization (data not shown).

DISCUSSION

Dorsal Hypodermal Cells Display Monopolar, Basolateral Protrusive Activity during Intercalation

Dorsal intercalation in *C. elegans* is a simple example of directed epithelial cell rearrangement. Because it involves the rearrangement of a small number of cells in a predictable, alternating pattern that is invariant from embryo to embryo (Williams-Masson *et al.,* 1998), dorsal intercalation should be particularly amenable to cellular and genetic analysis. Although dorsal intercalation is reminiscent of convergent extension of dorsal deep cells in vertebrates (reviewed in Keller *et al.,* 2000), it involves the rearrangement of epithelial cells, and hence the cellular and molecular mechanisms that regulate it may differ significantly

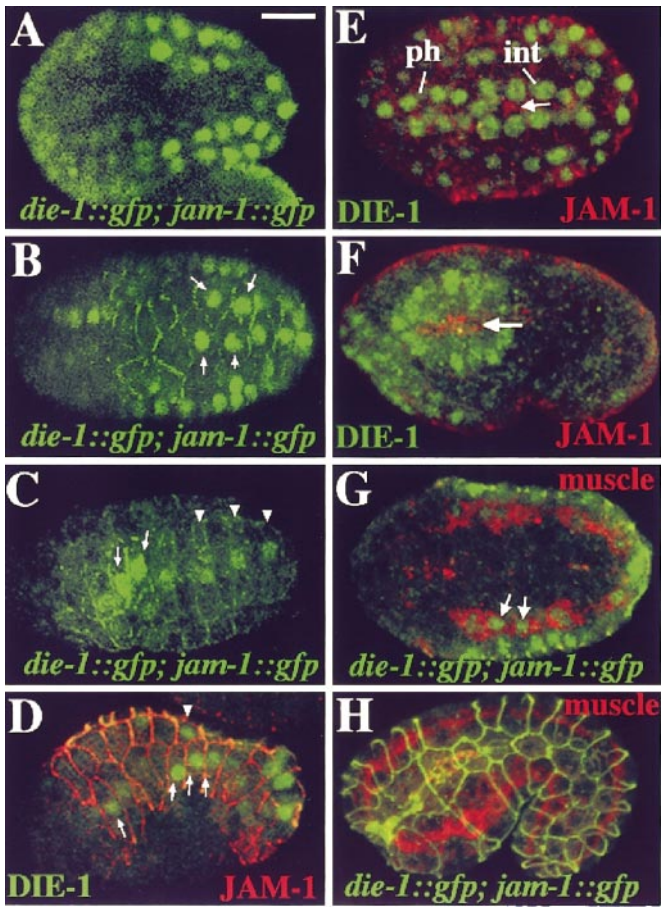

FIG. 8. DIE-1 expression. Confocal images were obtained of fixed wild-type embryos stained with anti-DIE-1 polyclonal antibodies (E, F) or of fixed homozygous *die-1(w34)* embryos expressing *DIE-1::GFP; JAM-1::GFP* from an extrachromosomal array, which were subsequently immunostained with anti-GFP antibodies (A–D, G, H; the signal represented by each channel is shown for each panel). (A) Middle focal plane of an embryo immediately prior to intercalation. Strong staining is observed in presumptive hypodermal precursors and muscle precursors. (B) An embryo during the early phase of dorsal intercalation. Note the elevated levels of DIE-1 in dorsal hypodermal nuclei (arrows). (C) An embryo near the completion of dorsal intercalation. DIE-1 expression has declined in posterior dorsal hypodermal cells (arrowheads), but is now higher in the "pointer cells," which are the last dorsal cells to intercalate (arrows). (D) Expression of DIE-1 (green) and JAM-1 (MH27 immunostaining, red) in lateral (arrowhead) and ventral (arrow) hypodermal cells (lateral view). (E) Expression of DIE-1 (green) in the pharyngeal (ph) and intestinal (int) primordia. DIE-1 is present in the nuclei of all gut cells; the lumen is identifiable by MH27 immunostaining (red, arrow). (F) Pharyngeal expression of DIE-1. An enclosed embryo immunostained for DIE-1 (green) and JAM-1 (red). Middle focal plane, lateral view. Arrow indicates JAM-1 expression associated with the epithelium lining the pharyngeal lumen. (G) An unenclosed embryo expressing *DIE-1::GFP; JAM-1::GFP* double stained with anti-GFP antibody (green) and muscle-specific antibody (red). *DIE-1::GFP* is detected in nuclei of muscle cells (arrows). (H) An enclosed embryo expressing *DIE-1::GFP; JAM-1::GFP* double stained with anti-GFP antibody (red) and a muscle-specific antibody (green). Epithelial cell junctions are observed in both channels (detecting *JAM-1::GFP*), but no nuclear GFP expression is observed, indicating *DIE-1::GFP* expression has ceased. Scale bar = 10 μm.

from those operating in deep cells. Our previous work (Williams-Masson *et al.*, 1998) showed that intercalating cells extend basolateral protrusions in the direction of rearrangement. Our dynamic analysis of dorsal intercalation using *gfp* translational fusions and multiphoton microscopy here confirms and extends this finding. As intercalation proceeds, basolateral protrusions become highly elongated medially; in contrast, we observed little protrusive activity at the lateral edges of intercalating cells.

Such highly asymmetric protrusive activity during intercalation is reminiscent of the "monopolar" protrusive activity exhibited by rearranging deep neural cells in the lateral neural plate of *Xenopus* (Elul and Keller, 2000). The signals that regulate such monopolar behavior are unclear. Monopolar protrusive activity in *Xenopus* deep neural cells requires persistent vertical interactions with the underlying mesoderm. In addition, monopolar protrusions are unable to cross the boundary between lateral and medial ("notoplate") neural cells (reviewed in Keller *et al.*, 2000). Whether similar stimulatory or repulsive cues exist in *C. elegans* is unclear. It is possible that local cell–cell signals mediate the initial polarization of dorsal hypodermal cells. If such signals operate, they must do so immediately after the terminal divisions of dorsal hypodermal precursors, given that monopolar behavior ensues within minutes after dorsal hypodermal cells are born. In contrast to *Xenopus* deep neural cells, our laser ablation studies and genetic mosaic analysis suggest that, once polarized, dorsal hypodermal cells perform many of the subsequent events of intercalation in a cell-autonomous manner (see below).

Defects in die-1(w34) Embryos Show That the Steps of Intercalation Are Genetically Separable into Early and Late Phases

die-1 is the first cloned gene that has been shown to be directly required for cell rearrangements within the dorsal hypodermis, and provides several insights into how dorsal intercalation is regulated, both temporally and spatially. Based on our multiphoton microscopic analysis, C-derived dorsal hypodermal cells appear normal in *die-1(w34)* mutants in several respects. First, they are correctly polarized along the right-left axis because they can extend polarized protrusions that initially appear indistinguishable from those of wild-type siblings. Second, because basolateral protrusions are initially extended in a normal fashion by C-derived mutant cells, the cytoskeletal machinery required for this process must function normally, at least initially. Third, the apical junctional domains of C-derived mutant cells become wedge-shaped, indicating that ini-

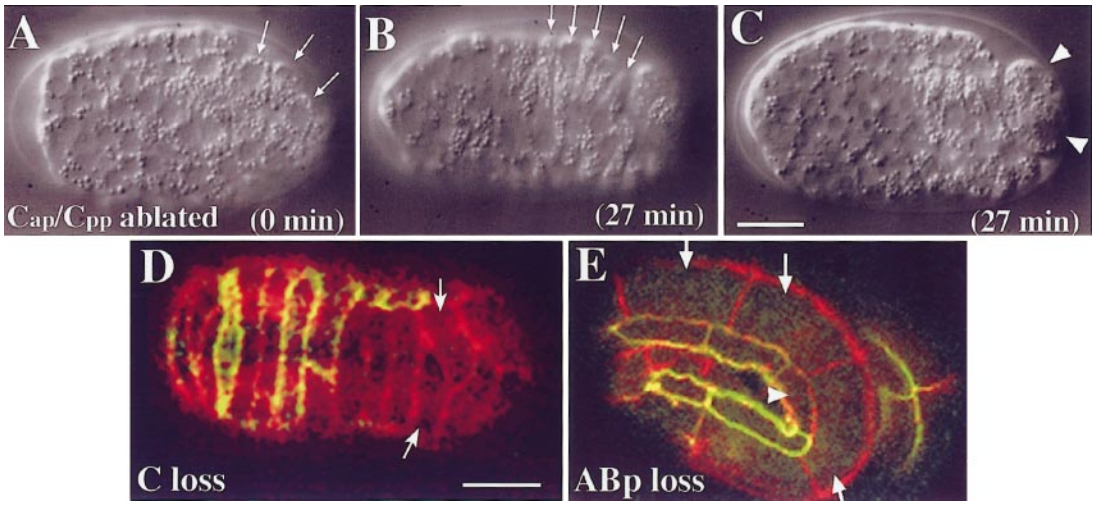

FIG. 9. Tissue-specific requirements for DIE-1. (A–C) Time course of development of a single wild-type embryo in which the muscle precursor cells Cap and Cpp were ablated (dorsal view). Despite the absence of about one-third of the body muscle (primarily posterior and dorsally positioned cells), intercalation occurs normally. Intercalating dorsal cells in A and B are indicated by arrows. (A) Start of intercalation. (B) Intercalation complete. (C) Interior focal plane; arrowheads indicate undifferentiated ablated material. Times indicate amount of time elapsed from the beginning of intercalation. (D) DIE-1 is required within progeny of C for their intercalation. Embryos from a homozygous *die-1(w34)* strain rescued by an extrachromosomal array expressing *DIE-1::GFP; JAM-1::GFP* were analyzed. Embryos were stained with anti-GFP antibody (green) and MH27 (red). Mosaic embryos were identified as embryos that showed normal MH27 staining in the red channel, but expressed *JAM-1::GFP* only in a subset of the epithelial cells in the green channel. No *JAM-1::GFP* expression is observed in the posterior dorsal hypodermis, which is derived from the C lineage and includes several unintercalated cells (arrows). AB-derived cells have intercalated normally. (E) Mosaic loss in ABp. This embryo elongated normally. Arrows indicate ventral hypodermal cells that are not expressing the array, based on the absence of signal in the green channel. Arrowhead indicates a lateral hypodermal cell that does not contain the array. Thorough analysis of the embryo showed that none of the ABp-derived hypodermal cells that could be analyzed contained the array, whereas all ABa-derived and non-AB cells that could be analyzed expressed the array. Scale bar = 10 μm.

tially the cells are capable of remodeling their apical junctions. However, the subsequent translocation of the cell body, which is crucial for successful completion of cell rearrangement, is defective in the mutants. How cell translocation occurs during dorsal intercalation is currently unknown. It is known that dorsal intercalation depends on both actin filaments and microtubules (Williams-Masson *et al.*, 1998); DIE-1 could regulate proteins required for cytoskeletal reorganization. It is also possible that cell–substrate or cell–cell interactions are affected in the mutant. It is known that the classical cadherin–catenin complex is not required for dorsal intercalation to occur (Costa *et al.*, 1998; Raich *et al.*, 1999), but little else is known about the changes that occur on the surface of migrating dorsal cells as they rearrange. Whatever molecules are regulated by DIE-1, our results demonstrate that

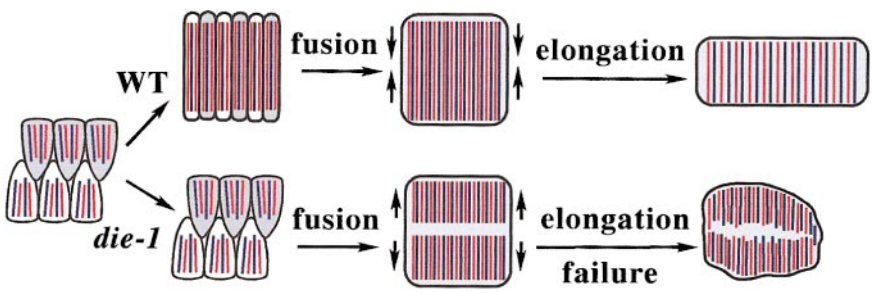

FIG. 10. A model for DIE-1 function during intercalation and elongation. Hypodermal cells produce arrays of cytoskeletal elements (red: actin; blue: microtubules) that become progressively aligned circumferentially as intercalation is completed and elongation begins. During elongation, loss of DIE-1 function results in incomplete intercalation, leading to failure of cytoskeletal elements to span the entire dorsal hypodermal array. After fusion, the cytoskeletal network is discontinuous at the dorsal midline, leading to elongation failure.

the process of epithelial cell rearrangement can be subdivided into several distinct steps in *C. elegans*. Moreover, since mutations in *die-1* affect only the later stages of intercalation, it should be possible to genetically dissect these temporally distinct phases of intercalation in *C. elegans*.

die-1 Encodes a Cell-Autonomous Regulator of Intercalation in Posterior Dorsal Hypodermal Cells

die-1 encodes a C2H2 zinc finger nuclear protein containing four zinc fingers. Elucidation of transcriptional targets of DIE-1 awaits further experiments. However, based on the lack of overt patterning defects in *die-1(w34)* homozygotes, we favor the hypothesis that DIE-1 regulates structural genes whose products are required for intercalation. In that *die-1* encodes a putative transcriptional regulator, it is likely that DIE-1 acts autonomously within the posterior dorsal hypodermis to regulate factors necessary for intercalation. Analysis of mosaic embryos in which *die-1* function was lost in progeny of the C blastomere supports this suggestion. In these embryos, with the exception of the anteriormost pair of C-derived dorsal cells, cells lacking DIE-1 fail to intercalate. Previous laser ablation experiments also support the view that dorsal cells, once polarized, intercalate in a predominantly autonomous fashion. Dorsal cells can intercalate in the absence of underlying muscle cells (our results), and our previous studies have shown that intercalation can occur in the absence of half of the lateral hypodermal cells or among anterior dorsal cells in the absence of posterior dorsal cells (Williams-Masson *et al.,* 1998). We infer from these experiments that the observed DIE-1 expression within the posterior muscle and lateral hypodermis is not required for dorsal intercalation because the cells themselves are dispensable.

Because DIE-1 is present in both posterior and anterior dorsal hypodermal cells, an obvious question arises: why are anterior dorsal hypodermal cells unaffected in *die-1(w34)* mutants? One possibility is that a lineage-restricted difference in regulatory pathways exists between AB- and C-derived hypodermal cells. If a second regulatory process operates in parallel with DIE-1 within the anterior, AB-derived dorsal cells, then intercalation could still occur in these cells despite the absence of DIE-1. That the boundary between dorsal hypodermal cells that can successfully intercalate and those that cannot corresponds to the boundary between AB- and C-derived dorsal hypodermis makes such lineage-specific regulatory differences a distinct possibility.

DIE-1 Is Required in Other Tissues That Undergo Directed Cell Rearrangement and Extension

In addition to defects in dorsal intercalation, *die-1(w34)* mutant embryos also display abnormalities in the processes of ventral enclosure, pharynx attachment, muscle organization, and gut formation. The presence of multiple morphogenetic defects in *die-1(w34)* mutants and the appearance of DIE-1 in each of the affected tissues suggest that DIE-1 may act to regulate multiple morphogenetic processes within the embryo. Our mosaic analysis is consistent with this view in the case of dorsal hypodermis (see above). However, it is also possible that some of the additional defects are secondary defects that arise because the process of intercalation has been perturbed. Our mosaic analysis identified one case in which such indirect defects may occur. We identified mosaic embryos that elongated completely normally yet displayed losses in the ABp lineage, which generates ventral hypodermal cells. This suggests that the ventral hypodermal defects associated with *die-1(w34)* mutants do not result from an autonomous requirement for DIE-1 within the ventral cells but, rather, are indirect.

In contrast to the ventral hypodermis, DIE-1 appears to be autonomously required in the gut. It is interesting to note that the cells within the *C. elegans* gut primordium undergo a type of intercalation (Leung *et al.,* 1999), although the process is somewhat different from that in the dorsal hypodermis. Failure of gut progenitors to intercalate properly could lead to a subsequent morphogenetic defect, including the detachment phenotype we observed in *die-1(w34)* mutants and offspring of *die-1(w34)* germline mosaic mothers. Although we did not recover mosaic animals in which a clean loss of DIE-1 function occurred within E, the gut progenitor cell, we did recover mosaics in which complex losses occurred that included E. In each case gut abnormalities were observed, consistent with an autonomous role for DIE-1 in the gut.

It is intriguing that the other tissues in which defects are observed in *die-1(w34)* mutants (i.e., pharynx and body wall muscle) also undergo coordinated changes in cell shape and position along a preferred axis. Muscle cells organize into quadrants and elongate along the anterior–posterior axis (reviewed in Moerman, 1997). Similarly, pharyngeal precursors, which arise as a ball of cells attached to the forming midgut, elongate anteriorly to connect to the buccal cavity (Portereiko and Mango, 2001). Although motile events in these tissues have not been examined carefully, they may involve processes that resemble intercalation. If this is the case, then DIE-1 may be a regulator of several similar morphogenetic processes in *C. elegans*.

Elongation Defects in die-1 Embryos May Result from Defects in Actin Filament Formation

Our analysis of the morphogenetic defects in *die-1(w34)* mutants sheds light on the consequences of intercalation for subsequent morphogenetic events. We have demonstrated defects in the actin cytoskeleton in *die-1(w34)* mutants. The defects in the cytoskeleton we observed could arise in several ways. One possibility is that DIE-1 indirectly regulates the reorganization of actin and microtubules in rearranging cells. A second possibility is that cytoskeletal disorganization in *die-1(w34)* mutants is a secondary result of the failure of dorsal hypodermal cells to intercalate. Although our results are consistent with either

possibility, we favor the latter. Elongation of *C. elegans* embryos is dependent on actin filaments that organize into a circumferential, uniformly spaced array within the hypodermis; distribution of actin-based contractile forces is thought to be mediated in part by microtubules (Priess and Hirsh, 1986; reviewed in Simske and Hardin, 2001). In *die-1(w34)* mutant embryos we observed organized actin and microtubules around the periphery of the dorsal syncytium, whereas the central region of the dorsal syncytium did not display organized, circumferentially organized filaments. That the cytoskeleton can organize to some extent in mutant embryos suggests that DIE-1 may not directly regulate filament formation per se; instead, the failure of cells to intercalate may prevent the cytoskeleton from aligning across the entire dorsal hypodermis. In this model, once intercalation is complete in wild-type embryos, cells span the width of the dorsal hypodermis, allowing the forming actin filaments and microtubules to stretch across the entire dorsal surface. In *die-1(w34)* mutants, individual polymers may be able to span the length of a cell, but if the cell fails to intercalate the individual filaments may not be able to span the entire dorsal hypodermis. In this case, the central area where the tips of cells were located might be expected to lack organized actin and microtubules (Fig. 10). Once the dorsal cells fuse, the actin and microtubule arrays would be interrupted by gaps at the dorsal midline; the lack of organized actin in turn could lead to defects during elongation.

The model we propose provides a role for intercalation in morphogenesis in *C. elegans* and suggests that intercalation events may be generally required for the production of columns of cells with aligned arrays of cytoskeletal elements that bear mechanical loads anisotropically. In this sense, the dorsal hypodermis is similar to the dorsal involuting marginal zone of *Xenopus.* Marginal zone cells that have undergone convergent extension are measurably stiffer along the anterior–posterior axis than those that have not (Moore *et al.*, 1995). Moore *et al.* (1995) proposed that tension-resisting elements (i.e., actin filaments) reinforce converging and extending cells mediolaterally (i.e., perpendicular to the axis of extension) as they rearrange, and that microtubules may bear compressive loads as the cells extend. We have provided direct evidence for defects in similar tension-resisting and compression-bearing elements within the hypodermis of *C. elegans* when directed cell rearrangement is disrupted. Thus, such mechanical changes in rearranging cells may be a feature common to both deep (nonepithelial) and epithelial cells. As this and other morphogenetic processes regulated by DIE-1 are unraveled, significant insights will be gained into the process of epithelial cell rearrangement. This in turn should deepen our understanding of this ubiquitous morphogenetic process.

ACKNOWLEDGMENTS

This work was supported by NSF Grant DBI97–24515 and NIH Grant GM58038 awarded to J.H., and NIH Grant GM48137 awarded to J.H.R. W.A.M. was supported by a NIH postdoctoral fellowship and a Development Grant from the Muscular Dystrophy Association. W.B.R. and P.J.H. were supported by a UW Molecular Biosciences Predoctoral Training grant (NIH T32-GM0721). We thank S. Segal for assistance with initial mapping experiments, K. Kopish for help with *ojEx3,* and J. Squirrell and J. G. White for access to the multiphoton optical workstation at the University of Wisconsin. We also thank members of the Hardin laboratory, especially T. Lindblom and J. Simske, for helpful discussion and critical reading of the manuscript.

REFERENCES

Blumenthal, T. (1995). Transsplicing and polycistronic transcription in *Caenorhabditis elegans. Trends Genet.* **11,** 132–136.

Brenner, S. (1974). The genetics of *Caenorhabditis elegans. Genetics* **77,** 71–94.

Brown, S., and Castelli-Gair Hombría, J. (2000). Drosophila *grain* encodes a GATA transcription factor required for cell rearrangement during morphogenesis. *Development* **127,** 4867–4876.

Burdine, R. D., Chen, E. B., Kwok, S. F., and Stern, M. J. (1997). *egl-17* encodes an invertebrate fibroblast growth factor family member required specifically for sex myoblast migration in *Caenorhabditis elegans. Proc. Natl. Acad. Sci. USA* **94,** 2433–2437.

Costa, M., Draper, B. W., and Priess, J. R. (1997). The role of actin filaments in patterning the *Caenorhabditis elegans* cuticle. *Dev. Biol.* **184,** 373–384.

Costa, M., Raich, W., Agbunag, C., Leung, B., Hardin, J., and Priess, J. R. (1998). A putative catenin-cadherin system mediates morphogenesis of the *Caenorhabditis elegans* embryo. *J. Cell. Biol.* **141,** 297–308.

Elul, T., and Keller, R. (2000). Monopolar protrusive activity: A new morphogenetic cell behavior in the neural plate dependent on vertical interactions with the mesoderm in Xenopus. *Dev. Biol.* **224,** 3–19.

Ettensohn, C. A. (1985). Gastrulation in the sea urchin embryo is accompanied by the rearrangement of invaginating epithelial cells. *Dev. Biol.* **112,** 383–390.

Ferguson, K. C., Heid, P. J., and Rothman, J. H. (1996). The SL1 trans-spliced leader RNA performs an essential embryonic function in *Caenorhabditis elegans* that can also be supplied by SL2 RNA. *Genes Dev.* **10,** 1543–1556.

Godt, D., and Laski, F. A. (1995). Mechanisms of cell rearrangement and cell recruitment in *Drosophila* ovary morphogenesis and the requirement of *bric a brac. Development* **121,** 173–187.

Goh, P. Y., and Bogaert, T. (1991). Positioning and maintenance of embryonic body wall muscle attachments in *C. elegans* requires the *mup-1* gene. *Development* **111,** 667–681.

Griffin, K. J., Amacher, S. L., Kimmel, C. B., and Kimelman, D. (1998). Molecular identification of *spadetail*: Regulation of zebrafish trunk and tail mesoderm formation by T-box genes. *Development* **125,** 3379–3388.

Hardin, J. (1989). Local shifts in position and polarized motility drive cell rearrangement during sea urchin gastrulation. *Dev. Biol.* **136,** 430–445.

Heisenberg, C. P., Tada, M., Rauch, G. J., Saude, L., Concha, M. L., Geisler, R., Stemple, D. L., Smith, J. C., and Wilson, S. W. (2000). Silberblick/Wnt11 mediates convergent extension movements during zebrafish gastrulation. *Nature* **405,** 76–81.

Irvine, K. D., and Wieschaus, E. (1994). Cell intercalation during *Drosophila* germband extension and its regulation by pair-rule segmentation genes. *Development* **120,** 827–841.

Keller, R., Davidson, L., Edlund, A., Elul, T., Ezin, M., Shook, D., and Skoglund, P. (2000). Mechanisms of convergence and extension by cell intercalation. *Philos. Trans. R. Soc. Lond. B Biol. Sci.* **355,** 897–922.

Keller, R., and Tibbetts, P. (1989). Mediolateral cell intercalation in the dorsal, axial mesoderm of *Xenopus laevis*. *Dev. Biol.* **131,** 539–549.

Keller, R. E. (1980). The cellular basis of epiboly: An SEM study of deep-cell rearrangement during gastrulation in *Xenopus laevis*. *J. Embryol. Exp. Morphol.* **60,** 201–234.

Keller, R. E., and Trinkaus, J. P. (1987). Rearrangement of enveloping layer cells without disruption of the epithelial permeability barrier as a factor in *Fundulus* epiboly. *Dev. Biol.* **120,** 12–24.

Kelly, W. G., and Fire, A. (1998). Chromatin silencing and the maintenance of a functional germline in Caenorhabditis elegans. *Development* **125,** 2451–2456.

Kim, S. H., Yamamoto, A., Bouwmeester, T., Agius, E., and Robertis, E. M. (1998). The role of paraxial protocadherin in selective adhesion and cell movements of the mesoderm during Xenopus gastrulation. *Development* **125,** 4681–4690.

Klug, A., and Rhodes, D. (1987). Zinc fingers: A novel protein fold for nucleic acid recognition. *Cold Spring Harb. Symp. Quant. Biol.* **52,** 473–482.

Leung, B, Hermann, G. J., and Priess, J. R. (1999). Organogenesis of the *Caenorhabditis elegans* intestine. *Dev. Biol.* **216,** 114–134.

Mello, C., and Fire, A. (1995). DNA transformation. *Methods Cell Biol.* **48,** 451–482.

Mello, C. C., Kramer, J. M., Stinchcomb, D., and Ambros, V. (1991). Efficient gene transfer in *C. elegans*: Extrachromosomal maintenance and integration of transforming sequences. *EMBO J.* **10,** 3959–3970.

Miller, D. M., and Shakes, D. C. (1995). Immunofluorescence microscopy. *Methods Cell Biol.* **48,** 365–394.

Moerman, D. G., and Fire, A. (1997). Muscle: Structure, function, and development. *In* "*C. elegans* II" (D. L. Riddle, T. Blumenthal, B. J. Meyer, and J. R. Priess, Eds.), pp. 417–470. Cold Spring Harbor Laboratory Press, Plainview, NY.

Mohler, W. A., Simske, J. S., Williams-Masson, E. M., Hardin, J. D., and White, J. G. (1998). Dynamics and ultrastructure of developmental cell fusions in the *Caenorhabditis elegans* hypodermis. *Curr. Biol.* **8,** 1087–1090.

Mohler, W. A., and White, J. G. (1998). Stereo-4-D reconstruction and animation from living fluorescent specimens. *Biotechniques* **24,** 1006–1012.

Moore, S. W., Keller, R. E., and Koehl, M. A. R. (1995). The dorsal involuting marginal zone stiffens anisotropically during its convergent extension in the gastrula of *Xenopus laevis*. *Development* **121,** 3131–3140.

Plenefisch, J., Xiao, H., Mei, B., Geng, J., Komuniecki, P. R., and Komuniecki, R. (2000). Secretion of a novel class of iFABPs in nematodes: Coordinate use of the *Ascaris/Caenorhabditis* model systems. *Mol. Biochem. Parasitol.* **105,** 223–236.

Podbilewicz, B., and White, J. G. (1994). Cell fusions in the developing epithelial of *C. elegans*. *Dev. Biol.* **161,** 408–424.

Portereiko, M. F., and Mango, S. E. (2001). Early morphogenesis of the *Caenorhabditis elegans* pharynx. *Dev. Biol.* **233,** 482–494.

Priess, J. R., and Hirsh, D. I. (1986). *Caenorhabditis elegans* morphogenesis: The role of the cytoskeleton in elongation of the embryo. *Dev. Biol.* **117,** 156–173.

Ptashne, M. (1988). How eukaryotic transcriptional activators work. *Nature* **335,** 683–689.

Raich, W. B., Agbunag, C., and Hardin, J. (1999). Rapid epithelial-sheet sealing in the Caenorhabditis elegans embryo requires cadherin-dependent filopodial priming. *Curr. Biol.* **9,** 1139–1146.

Raich, W. B., Moran, A. N., Rothman, J. H., and Hardin, J. (1998). Cytokinesis and midzone microtubule organization in Caenorhabditis elegans require the kinesin-like protein ZEN-4. *Mol. Biol. Cell.* **9,** 2037–2049.

Sambrook, J., Fritsch, E. F., and Maniatis, T. (1989). "Molecular Cloning: A Laboratory Manual," 2nd ed. Cold Spring Harbor Laboratory Press, Plainview, NY.

Schoenwolf, G. C., and Alvarez, I. S. (1989). Roles of neuroepithelial cell rearrangement and division in shaping of the avian neural plate. *Development* **106,** 427–439.

Schuh, R., Aicher, W., Gaul, U., Cote, S., Preiss, A., Maier, D., Seifert, E., Nauber, U., Schroder, C., Kemler, R., *et al.* (1986). A conserved family of nuclear proteins containing structural elements of the finger protein encoded by Kruppel, a *Drosophila* segmentation gene. *Cell* **47,** 1025–1032.

Simske, J. S., and Hardin, J. (2001). Getting into shape: Epidermal morphogenesis in Caenorhabditis elegans embryos. *Bioessays* **23,** 12–23.

Sulston, J. E., Schierenberg, E., White, J. G., and Thomson, J. N. (1983). The embryonic cell lineage of the nematode *Caenorhabditis elegans*. *Dev. Biol.* **100,** 64–119.

Tada, M., and Smith, J. C. (2000). *Xwnt11* is a target of *Xenopus Brachyury*: Regulation of gastrulation movements via dishevelled, but not through the canonical Wnt pathway. *Development* **127,** 2227–2238.

Wallingford, J. B., Rowning, B. A., Vogeli, K. M., Rothbacher, U., Fraser, S. E., and Harland, R. M. (2000). Dishevelled controls cell polarity during *Xenopus* gastrulation. *Nature* **405,** 81–85.

Warga, R. M., and Kimmel, C. B. (1990). Cell movements during epiboly and gastrulation in zebrafish. *Development* **108,** 569–580.

Williams, B. D., Schrank, B., Huynh, C., Shownkeen, R., and Waterston, R. H. (1992). A genetic mapping system in *Caenorhabditis elegans* based on polymorphic sequence-tagged sites. *Genetics* **131,** 609–624.

Williams-Masson, E. M., Heid, P. J., Lavin, C. A., and Hardin, J. (1998). The cellular mechanism of epithelial rearrangement during morphogenesis of the *Caenorhabditis elegans* dorsal hypodermis. *Dev. Biol.* **204,** 263–276.

Williams-Masson, E. M., Malik, A. N., and Hardin, J. (1997). An actin-mediated two-step mechanism is required for ventral enclosure of the *C. elegans* hypodermis. *Development* **124,** 2889–2901.

Wilson, P., and Keller, R. (1991). Cell rearrangement during gastrulation of *Xenopus*: Direct observation of cultured explants. *Development* **112,** 289–300.

Wilson, R., Ainscough, R., Anderson, K., Baynes, C., Berks, M., Bonfield, J., Burton, J., Connell, M., Copsey, T., Cooper, J., *et al.* (1994). 2.2 Mb of contiguous nucleotide sequence from chromosome III of *C. elegans*. *Nature* **368,** 32–38.

Yamamoto, A., Amacher, S. L., Kim, S. H., Geissert, D., Kimmel, C. B., and De Robertis, E. M. (1998). Zebrafish paraxial protocadherin is a downstream target of spadetail involved in morphogenesis of gastrula mesoderm. *Development* **125,** 3389–3397.

Received for publication March 7, 2001
Revised May 3, 2001
Accepted May 3, 2001
Published online June 22, 2001